MDPI

Article

Comparative Assessment of UAV and Sentinel-2 NDVI and GNDVI for Preliminary Diagnosis of Habitat Conditions in Burunge Wildlife Management Area, Tanzania

Lazaro J. Mangewa [1,2,*], Patrick A. Ndakidemi [1], Richard D. Alward [3], Hamza K. Kija [4], John K. Bukombe [4], Emmanuel R. Nasolwa [1] and Linus K. Munishi [1]

[1] School of Life Sciences and Bio-Engineering (LISBE), Nelson Mandela African Institution of Science and Technology, Arusha P.O. Box 447, Tanzania; patrick.ndakidemi@nm-aist.ac.tz (P.A.N.); immarich90@gmail.com (E.R.N.); linus.munishi@nm-aist.ac.tz (L.K.M.)
[2] College of Forestry, Wildlife and Tourism (CFWT), Sokoine University of Agriculture (SUA), Morogoro P.O. Box 3009, Tanzania
[3] Aridlands, LLC, Grand Junction, CO 81507, USA; ralward@aridlands-nrc.com
[4] Tanzania Wildlife Research Institute (TAWIRI), Arusha P.O. Box 661, Tanzania; hamza.kija@tawiri.or.tz (H.K.K.); bukombe.john@tawiri.or.tz (J.K.B.)
[*] Correspondence: mangewal@nm-aist.ac.tz

Abstract: Habitat condition is a vital ecological attribute in wildlife conservation and management in protected areas, including the Burunge wildlife management areas in Tanzania. Traditional techniques, including satellite remote sensing and ground-based techniques used to assess habitat condition, have limitations in terms of costs and low resolution of satellite platforms. The Normalized Difference Vegetation Index (NDVI) and Green NDVI (GNDVI) have potential for assessing habitat condition, e.g., forage quantity and quality, vegetation cover and degradation, soil erosion and salinization, fire, and pollution of vegetation cover. We, therefore, examined how the recently emerged Unmanned Aerial Vehicle (UAV) platform and the traditional Sentinel-2 differs in indications of habitat condition using NDVI and GNDVI. We assigned 13 survey plots to random locations in the major land cover types: three survey plots in grasslands, shrublands, and woodlands, and two in riverine and mosaics cover types. We used a UAV-mounted, multi-spectral sensor and obtained Sentinel-2 imagery between February and March 2020. We categorized NDVI and GNDVI values into habitat condition classes (very good, good, poor, and very poor). We analyzed data using descriptive statistics and linear regression model in R-software. The results revealed higher sensitivity and ability of UAV to provide the necessary preliminary diagnostic indications of habitat condition. The UAV-based NDVI and GNDVI maps showed more details of all classes of habitat conditions than the Sentinel-2 maps. The linear regressions results showed strong positive correlations between the two platforms ($p < 0.001$). The differences were attributed primarily to spatial resolution and minor atmospheric effects. We recommend further studies to test other vegetation indices.

Keywords: remote sensing; Unmanned Aerial Vehicle; vegetation indices; wildlife habitats; satellite platforms; ecological monitoring

1. Introduction

Wildlife habitat condition is a cornerstone of conservation and management. Habitat degradation and loss are a major threat to conservation worldwide manifested by reduction or loss of requirements such as forage resources (quantity and quality) for wild herbivores. Forage resources include biomass materials for herbivores in landscapes [1,2], which may vary considerably in quantity and quality at different spatiotemporal scales across landscapes [3,4]. However, forage resources are crucial for attracting and sustaining wild herbivores in protected areas [3,5–7] due to their impact on the survival and reproduction of wild herbivores [8–11].

The degradation and loss of wildlife habitat in many protected and adjacent areas is largely attributed to human-induced land use and land cover changes (LULC) [12]. Land degradation is described as "how one or more land resources (soil, water, vegetation, rocks, air, climate, and relief) have changed for the worse" [13]. These threats impose significant challenges to wildlife management, including the increased risk of human–wildlife conflicts when herbivores stray beyond the protected area boundaries in search of resources [14,15]. This habitat degradation and loss also leads to the over-utilization of the few areas having the required resources, impairing the ecological integrity and potential utility of entire protected areas [4,16].

A vital starting point for monitoring wildlife habitat conditions and other ecological aspects is the status of land cover, which provides information on habitat availability, from local areas to landscape levels and beyond [17]. Land cover is defined as a biophysical feature that covers the earth's surface [14,17,18]. It influences habitat conditions that affect the abundance, diversity, and distribution of wildlife species [14,17].

Different vegetation indices, including Normalized Difference Vegetation Index (NDVI) and its advanced version, Green NDVI (GNDVI), have been developed to provide information on the status of land cover and trends in land cover changes, such as degradations that reflect impacts on forage quantity and quality [7,14,17]. However, many studies, including those that have used the NDVI and GNDVI, have directly focused on one or a few elements of land degradation or habitat condition in conservation areas, such as vegetation cover change [17–19], forage quantity and quality [7,9], soil erosion and salinization [14,20,21], and effects of wildfire and pollutants on vegetation cover [14,22]. None of these studies assessed the preliminary indicative information about the targeted habitats where conditions seemed abnormal.

Traditional methods used to assess and monitor wildlife habitat conditions include ground survey techniques and satellite aerial remote sensing platforms. These methods have well-recognized shortcomings. For example, ground-based techniques are laborious, costly [23], and challenging in poorly accessible areas. Additionally, freely available satellite imagery has low spatial resolutions, making this approach unable to detect habitat change that may be significant to wildlife. Since early detection of changing habitat condition is essential, clear preliminary signals from an effective platform are vital for timely solutions to specific environmental problems. For large areas, ground-based quantification of habitat conditions such as available forage for herbivores is less practical, whereas vegetation indices such as NDVI are useful [24]. The use of Unmanned Aerial Vehicles (UAVs) to collect NDVI data at a high resolution (e.g., 0.01 to 0.1 m) may be the solution [23,25].

The most widely used vegetation index for habitat conditions is NDVI. Uses of NDVI include the study by Carella et al. [26], who monitored the canine distemper virus (CDV) and habitat fragmentations; Soria et al. [27], who monitored subaquatic vegetation in lakes; and Shamsudeen et al. [28], who assessed vegetation health. Its strengths lie in its capability to lessen noise arising from cloud shadows, variations in topographic levels, and different illumination intensities [29–31]. However, one of its weaknesses is that it saturates at higher Leaf Area Index (LAI), reducing its ability to distinguish between high and very high LAI [30,32]. These limitations necessitated a second and advanced vegetation index, GNDVI, that provides valuable information on complex landscapes [4]. For instance, GNDVI has a high sensitivity to chlorophyll and reduces non-photosynthetic effects [31,33–36]. Indices such as the Atmospherically Resistant Vegetation Index (ARVI), which are designed to counteract the challenges that face NDVI, have their own challenges, for instance, being highly sensitive to the soil reflectance effect; hence, this index is not appropriate for arid and semi-arid areas [32,37].

The application of a recently emerged UAV aerial remote sensing platform has yet to be scaled up to assess wildlife habitat in large, protected areas. Many studies, especially in African countries, have used UAVs in small areas such as farms and in a single or only a few vegetation cover types (e.g., grassland or forest). For instance, Matese et al. [38] focused on a vineyard, assessing the variability of vine parameters using UAV-and-Sentinel-based

NDVI. The authors noted the possible loss of crucial information and misinterpretation of NDVI from mixed pixels. Sozzi et al. [39], also focused on a few vineyard blocks. The authors noted a non-transferable finding for blocks with inter-row vegetation growth such as grass to those with no grass. A recent systematic review by Haula and Agbozo [40] shows that "UAV adoption in the sub-region is still in its early phase in Africa, with several implemented cases primarily focusing on healthcare and crop farming". Although UAVs are gradually being adopted in research across Africa, from Senegal to South Africa [19,40–43], none have included multiple land cover types in a single study. Furthermore, no study has used this technology to address large landscapes with heterogeneous land cover types within Tanzania. Instead, Tanzanian researchers have narrowly focused on crop yields [44], detecting chimpanzee nests [45], detecting erosion and topographical changes [46], or changes in a single wetland and river basin [38]. Therefore, we explored the levels at which UAV and Sentinel-2 provide crucial preliminary signals of habitat conditions using NDVI and GNDVI as the indicators. The study was crucial to ascertain the potential of a recently emerged UAV technology for real-time preliminary signals of detection and monitoring of habitat conditions in the Burunge Wildlife Management Area (WMA) which faces many threats, including livestock grazing and cultivation that compete with wild herbivores [39]. The Burunge WMA has been a protected area in Tanzania since 2003 with a focus on conserving biodiversity and natural and cultural resources while contributing to the local livelihoods of the communities [47]. Since it is not as large as the core protected area of Tarangire and Lake Manyara National Parks that it abuts, UAV technology could help monitor the habitat conditions within and adjacent to it.

Specifically, we aimed to compare initial, quantitative indicator values of habitat conditions based on NDVI and GNDVI values derived from the two platforms in each land cover type. We also aimed to compare the two platforms based on NDVI and GNDVI maps as spatial-visual distribution patterns of the preliminary habitat condition levels (i.e., very good, good, poor, and very poor). We ultimately aimed to test if there was a statistically significant difference between the preliminary indications of habitat conditions based on the NDVI and GNDVI generated by UAV and Sentinel-2. The levels of habitat condition in different land cover types reflect the likelihood of habitats attracting wild herbivores. This is important to enable wildlife managers and ecologists to quickly collect environmental data over large areas which indicate possible ecological problems. This step can help wildlife managers to take appropriate habitat improvements and management measures [29], and plan for the needed resources to monitor and address site-specific or landscape problems and possible causes. The urgent need for timely and accurate information based on powerful aerial remote sensing platforms for an appropriate detection and monitoring any disturbances and changes in landscapes has also been recently reported by Sumari et al. [48,49].

2. Materials and Methods

2.1. Study Area

The Burunge WMA is a 243 km^2 community-based conservation area located at the interphase between Lake Manyara and Tarangire National Parks in the northern tourism circuit of Tanzania (Figure 1). The WMA was established in 2003 by ten villages (Minjingu, Mwada, Vilima Vitatu, Sangaiwe, Magara, Manyara, Maweni, Ngoley, Kakoi, and Olasity). Each village contributed a portion of its land, guided by land use plans, for conservation and socio-economic benefits, following the Wildlife Management Areas Regulations of 2002 (Revised in 2012) [50]. The WMA is an ecologically crucial migratory wildlife corridor for African elephants (*Loxodonta africana*), wildebeest (*Connochaetes taurinus*), and zebra (*Equus quagga*), and serves as a protected buffer area for many other wildlife species from the neighboring protected areas.
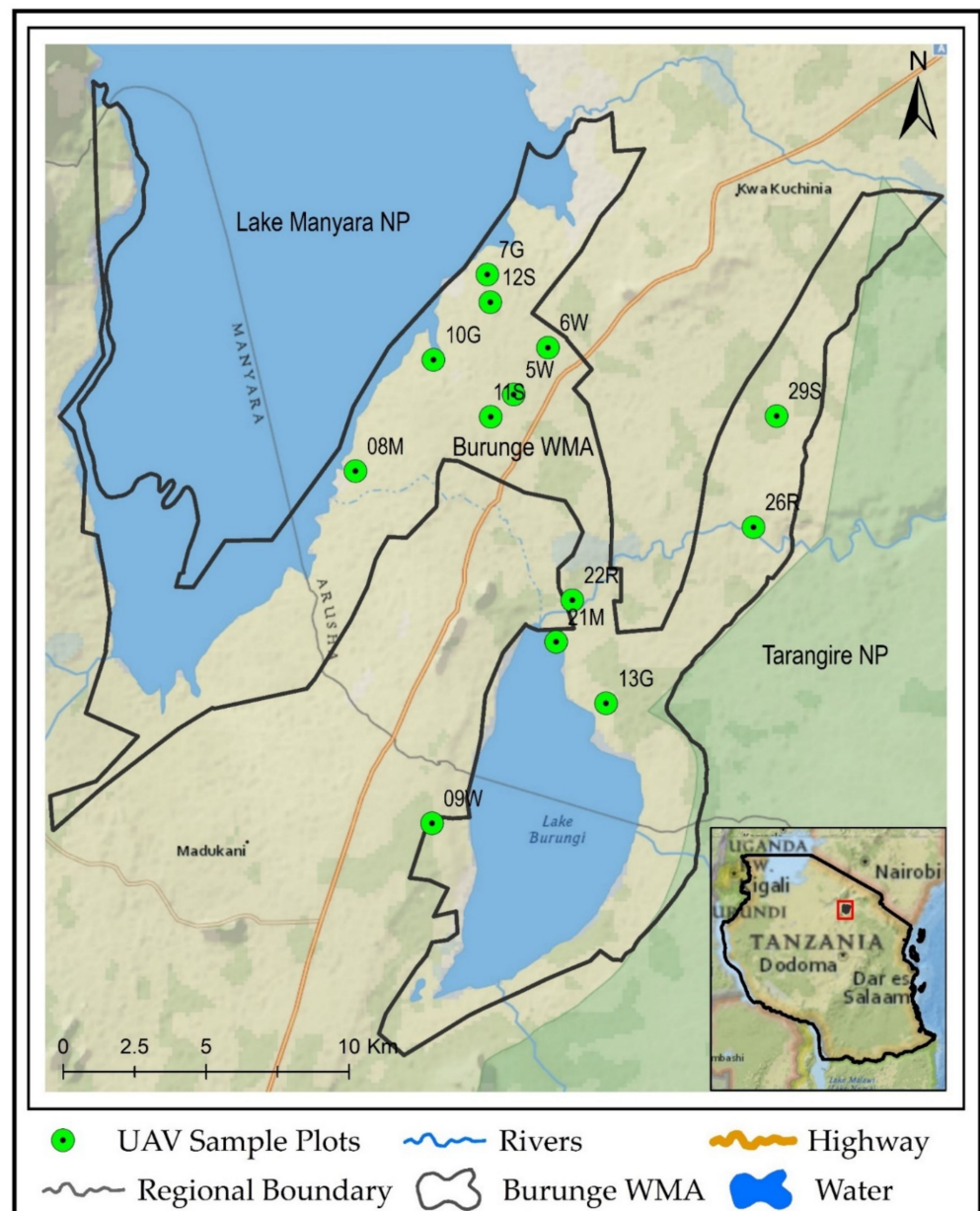
Figure 1. A map of Burunge WMA showing its location and surveyed plots in different land cover types; grassland (7G, 10G and 13G), shrubland (11S, 12S and 29S), woodland (5W, 6W and 09W), riverine (22R and 26R), and mosaic (08M and 21M).

The Burunge WMA is characterized by woodland, shrubland, grassland, riverine vegetation, mixed vegetation (termed "mosaic" in this study), water, bare ground, and agriculture. Agriculture is practiced illegally along the boundary and in small areas within the WMA. The WMA's annual rainfall ranges between 400 and 650 mm. The rains fall in two seasons: the short-rainy season spans between November and February, while the heavy rainy season is between March and May [51]. The mean annual temperature ranges between 8 °C and 33 °C, depending on elevation [52,53]. The WMA's elevation is 1000 m above sea level (m.a.s.l.). Tarangire River is the only permanent primary source of freshwater for wildlife and livestock in the Tarangire–Manyara ecosystem [53]. Lakes Manyara and Burunge in the ecosystem are among the top saline-alkaline lakes in the East African Rift Valley system [54].

2.2. Data Collection

2.2.1. Sample Plots and Flight Mission Planning

We stratified the study area based on the existing main land cover types that have been previously documented [55,56]. These cover types were confirmed on the ground using expert knowledge and experience aided by high-resolution google earth images. Our study focused on and selected survey plots in the grassland, shrubland, woodland, riverine, and mosaic land cover types. The forest cover type located at one extreme narrow end along Lake Manyara was not selected due to logistic constraints. From the aerial proportions of land cover types generated by another research component under the same project, we purposively assigned 13 survey plots to random locations after stratifying the study area based on the major land cover types: three survey plots in grasslands, shrublands, and woodlands, and two in riverine and mosaics cover types, respectively (Figure 1).

A hand-held Garmin CSX GPS was used to trace the selected survey plots. We adjusted survey plots falling in inaccessible areas (due to terrain features or the absence of roads) by selecting nearby pixels with similar characteristics. We then used Yuneec's DataPilot planner for UAV flight mission planning. In each plot, the percentage cover and critical species composition of three layers (tree, shrub, and grasses/herbaceous) were determined following Braun-Blanquet [57] by another research component under the same project [58] (Figure 2). In large landscapes, the percentage cover of plant species in each layer is linked to the habitat condition in terms of forage cover for herbivores [59].

Figure 2. Researchers updating land cover types of Burunge WMA partly using the ground sampling scheme re-drawn from Braun-Blanquet [57] and UAV orthoimages under the other concurrent research component under this project. Some plots were within the UAV flight mission plans for this output. The "a" is a 4 m^2 sub-plot nested within "b", a 400 m^2 sub-plot nested within "c", 2500 m^2 main plot that was randomly placed in a nearly uniform vegetation cover "d". To the right is a photo taken in one 2500 m^2 large plot demarcated using a tape measure [58].

2.2.2. Acquisition of Satellite Imagery

Sentinel-2 imagery was obtained close to the UAV flight dates (February–March 2020) to ensure an appropriate match of the values of vegetation indices derived from the two platforms [4]. We used satellite imagery with minimal cloud cover (<5%) acquired between the short rains and the commencement of the wet season (February–March 2020) from the United States Geological Survey web portal (https://www.usgs.gov/, acquired on: 21 February 2020).

The WMA is covered by only two Sentinel-2 tiles, downloaded from the Sentinel-2 ID: 36 MYA (Centroids: Latitude −4.1118 and Longitude 35.2956, acquired on: 21 February 2020) and 36 MZA (Centroids: Latitude −4.1087 and Longitude 36.1956, acquired on: 8 February 2020) (https://scihub.copernicus.eu/). The raw images were pre-processed in ERDAS Imagine 2015, and the corresponding NDVI and GNDVI extractions were performed in ArcGIS 10.8, following standard flow and procedures shown in the data processing Section 2.3 below.

2.3. Data Processing

This stage followed a systematic flow of steps to generate data from the UAV-orthoimages and Sentinel-2 imagery for each land cover type for statistical analysis (Figure 3). To test the detection effectiveness in different land cover types in the Burunge WMA, we employed the NDVI and GNDVI indices. We compared the two indices by analyzing the UAV images captured between 26 February and 13 March 2020 with a time-matched Sentinel-2 satellite.
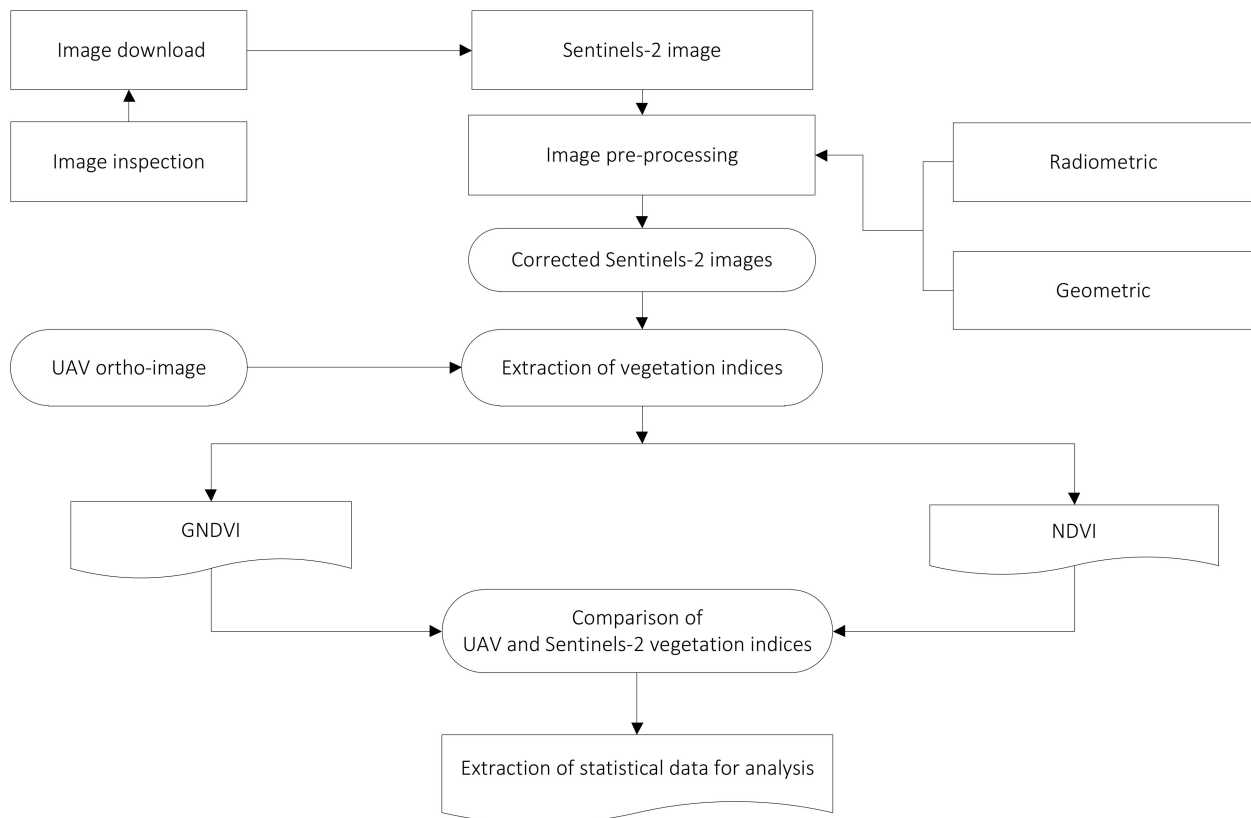

Figure 3. Flow chart demonstrating image processing and data extraction.

2.3.1. UAV-Based Image Acquisition in the Field

Before the actual fieldwork for UAV-based data collection, we registered the UAV and secured all the necessary permits per the Tanzania Civil Aviation (Remotely Piloted Aircraft Systems) Regulations, 2018 [60]. We also observed ethics and accessed permits at the community level and Local Government Authority [60,61].

We used a hexacopter UAV (H520, Yuneec Americas, Santa Clara, CA, USA) outfitted with payloads that included a 5-band multispectral camera (RedEdge3, MicaSense, Washington, DC, USA) (Figure 4). The RedEdge3 band characteristics facilitated direct satellite comparisons (Table 1). We accomplished the radiometric calibration through two means. First, each mission started by capturing a manual image of a standardized reflectance panel (RP02, MicaSense, Seattle, WA, USA). Second, an upward-facing down-welling light sensor (DLS-1, MicaSense, Seattle, WA, USA) recorded the lighting conditions which were incorporated into the metadata of each image capture. All flight missions were conducted at an altitude of 120 m above ground level (AGL) at a constant speed of 5 m/s along predefined flight lines, capturing images in an auto-pilot mode at 2 s interval with 75% front and 65% side overlaps. Each image measured approximately 8295 m^2 on the ground, achieving an average ground sampling distance (GSD), and pixel size, of about 8.5 cm. The Regular RGB camera (E90_8.3_4864 × 3648) generated images with an average GSD of 3.34 cm. All UAV imagery collections were executed within ±2 h of solar noon and

completed between 24–26 February and 11–13 March 2020. Our study was limited to this period, similar to the survey by Sozzi et al. [39].
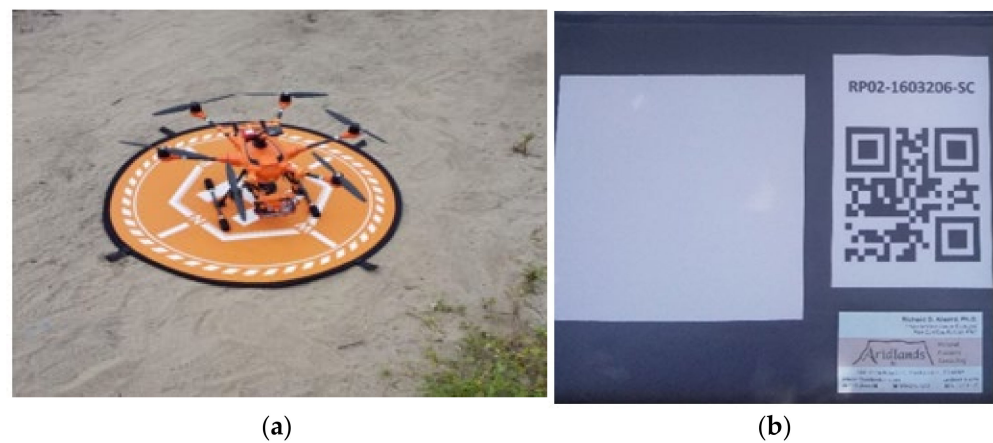
Figure 4. UAV Yuneec H520 (**a**) and a standard reflectance panel (RP02, MicaSense, Washington, DC, USA) (**b**).

Table 1. Band characteristics for the RedEdge3 multispectral camera and the Sentinel-2 multispectral imagery.

| Band Name | RedEdge3 | | | Sentinel-2 | | |
| | Wavelength (nm) | | | Wavelength (nm) | | |
	Band Number	Center	Width	Band Number	Center	Width
Blue	1	475	20	2	490	10
Green	2	560	20	3	560	10
Red	3	668	10	4	665	10
Near Infrared (NIR)	5	842	40	8	842	10
RedEdge	4	717	10	5	705	20

2.3.2. Extraction of NDVI and GNDVI Values from UAV-Based Orthoimages

We used Pix4Dmapper (ver. 4.5.6, Pix4D S.A., Prilly, Switzerland) for the mosaicking process for multispectral images acquired by UAV remote sensing aerial platform. We completed three processing steps: (i) initial processing; (ii) point cloud and mesh densification, and (iii) generation of Digital Surface Model (DSM), Orthomosaic, and a computation of indices. The Datum World Geodetic System-WGS 84, and UTM zone 37S, were selected as image geolocation and output Coordinate Systems, respectively, with a standard geolocation accuracy and auto-detection options.

2.3.3. Processing of Sentinel-2 Imagery and Extracting Vegetation Indices

We corrected the images for geometric and radiometric effects to remove a false indication of any object [62–66]. The Digital Elevation Model (DEM) at a 30 m resolution, derived from the Shuttle Radar Topography Mission (SRTM), corrected topographic effects on images that could affect the spatial distribution of vegetation types [67,68]. We analyzed the updated images to extract NDVI and GNDVI values based on accepted formulae (Table 2). We clipped the image locations and sizes from Sentinel-2 that matched the UAV-based ground sampling plots in ArcGIS 10.8 and extracted the pixels' corresponding values for statistical analysis.

Table 2. Vegetation indices used in the study *.
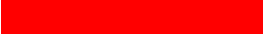
Vegetation Index	Formula		References
Normalized Difference Vegetation Index (NDVI)	$\text{NDVI} = \frac{\text{NIR} - \text{Red}}{\text{NIR} + \text{Red}}$	(1)	[33,69]
Green NDVI (GNDVI)	$\text{GNDVI} = \frac{\text{NIR} - \text{Green}}{\text{NIR} + \text{Green}}$	(2)	[34,35,37].

* Additional vegetation indices explored included EVI (Enhanced Vegetation Index [31,33,41–43,70]), EVI2 (Two Band EVI [33,42,43], RENDVI (Red Edge NDVI [44,45]), and WDRVI (Wide Dynamic Range Vegetation Index [46]) (Appendix A, Table A1).

2.3.4. Determination of NDVI and GNDVI Classes Using Scale Values

We calculated NDVI and GNDVI values from the multispectral images obtained from UAV and Sentinel-2 platforms [38] and categorized them into habitat condition classes (very good, good, poor, and very poor). The matching vegetation index color patterns at nine levels depicted the habitat condition classes along the color scale divided into 0.1-unit widths from 0.0 to 1.0. (Table 3). The colors distinguished four categories at specific levels: very good = 4 levels of green and blue, good = 2 levels of gold and yellow, poor = 2 levels of red and orange, and very poor= brown (Table 3). The established cut-off points for each class were generally agreed upon interpretations in line with those from "Agricolus" (https://www.agricolus.com/en/indici-vegetazione-ndvi-ndmi-istruzioni-luso/) and the Earth Observing System (EOS). We modified the color scale patterns based on published resources [23,71].

Table 3. Ranges of NDVI and GNDVI values for habitats condition classes.

Class	Colour	NDVI	GNDVI
Very Good		>0.9	> 0.8
		>0.8–0.9	>0.7–0.8
		>0.7–0.8	>0.6–0.7
		>0.6–0.7	>0.5–0.6
Good		>0.5–0.6	>0.4–0.5
		>0.4–0.5	>0.3–0.4
Poor		>0.3–0.4	>0.2–0.3
		>0.2–0.3	>0.1–0.2
Very Poor		≤0.2	≤0.1

2.4. Data Analysis

We checked the normality of data distribution using a Q-Q-test followed by descriptive statistics and linear regression model (R^2) in R-software (version 3.4.1) [72]. We ran a linear regression model in each land cover to test the statistical strengths of the link between the UAV and Sentinel-2 derived vegetation indices [38,39,73], as preliminary signals for habitat conditions. The test has been considered an appropriate spatial measure of any existing statistical bivariate association of data values between two variables [38].

3. Results

3.1. Comparative Results from UAV-and Sentinel-2 VI Histograms and Basic Statistics

The results in the histograms for NDVI and GNDVI values provide visualized levels of habitat conditions in each land cover type (Figure 5a,b). The color codes and respective vegetation index scales depict the different indicative levels of habitat conditions for NDVI (very good: >0.6–> 0.9; good: >0.4–0.6; poor: >0.2–0.4; and very poor: ≤0.2) and GNDVI (very good: >0.5–>0.8; good: >0.3–0.5; poor: >0.1–0.3; and very poor: ≤0.1). The UAV-based histograms indicate higher levels of good condition (>0.4–0.6) and very good condition (>0.6–0.9) than Sentinel-2 (Figure 5a). Sentinel-2 platform hardly detected the highest level

(>0.8–0.9) of the very good condition class but did signal habitat at the good condition class (>0.3–0.5) and the very good class (>0.5–0.8) using GNDVI (Figure 5b).
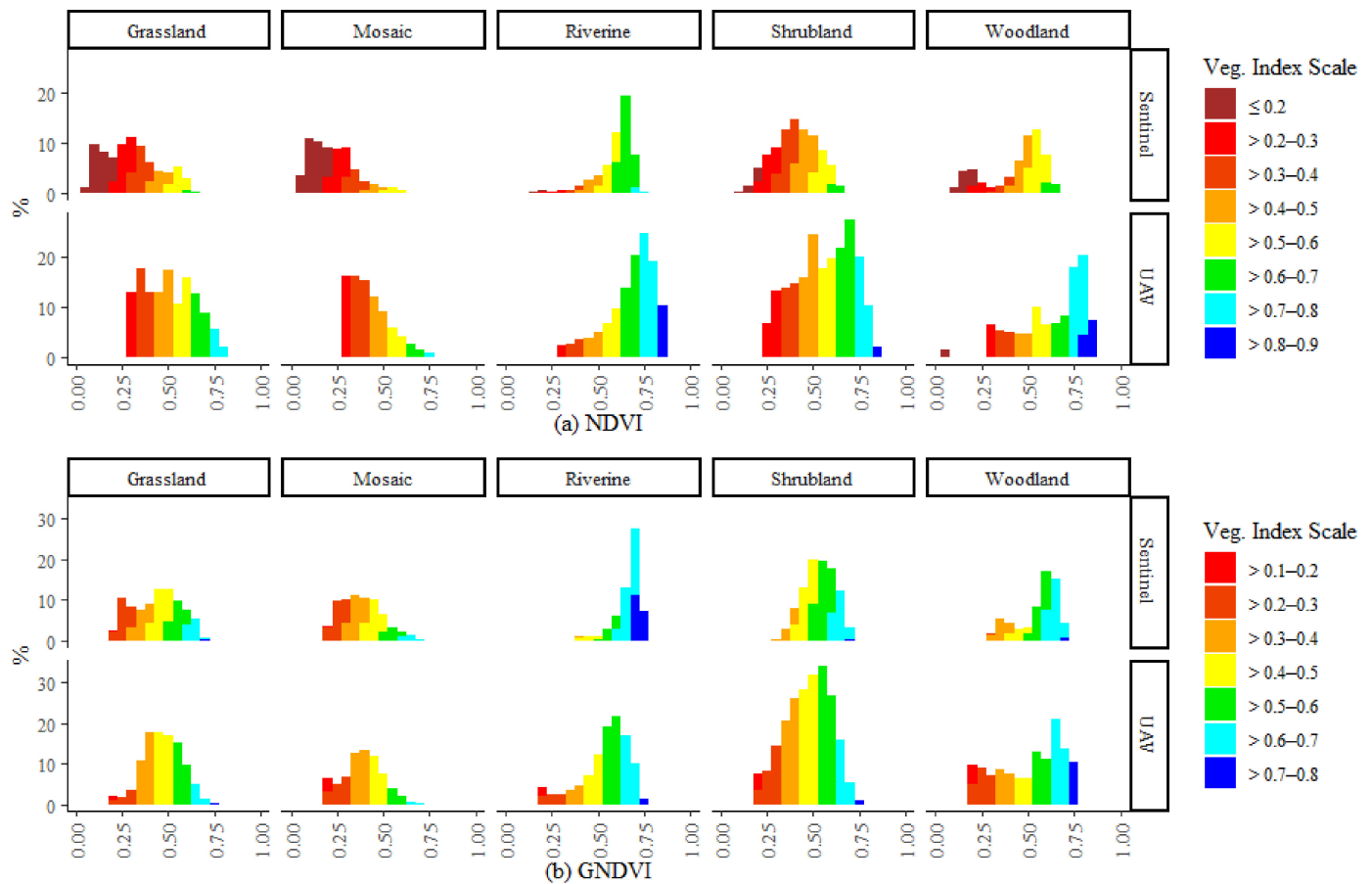
Figure 5. Frequency distribution of NDVI (**a**) and GNDVI (**b**) values to show visualized differences between UAV and GNDVI in providing preliminary signals of habitat conditions.

There were highly significant differences in mean habitat condition between the two platforms. Mean NDVI values for habitat condition were 0.09 to 0.20 higher for UAV-derived imagery for each land cover type compared to the Sentinel-2 platform (Table 4). We observed a lower coefficient of variation (CV) for UAV-based NDVI values than those generated using the Sentinel-2 platform for the grassland, mosaic, and woodland land cover types.

Similarly, mean GNDVI values for habitat condition were 0.02 to 0.07 higher when calculated from imagery derived from UAVs than those derived from the Sentinel-2 platform (Table 5). Additionally, we observed higher CV values for the UAV data than those from the Sentinel-2 in the riverine, shrubland, and woodland cover types. On the other hand, the UAV indicated a slightly lower CV for the GNDVI mean values in grassland and mosaic land cover types. One-way analysis of variance (ANOVA) using an F-test of the NDVI and GNDVI mean values derived from both UAV and Sentinel-2 within each land cover type revealed statistically significant variations between the platforms ($p < 0.001$).

3.2. Vegetation Index Maps

The vegetation index maps (NDVI and GNDVI) provided a clear spatial distribution pattern of habitats with very good, good, poor, and very poor condition classes in each land cover type derived from UAV orthoimages and Sentinel-2 imagery as indicated in Figure 6 and Supplementary Materials (Figures S1–S10). The UAV-based NDVI and GNDVI showed more variation and more detail of all the classes of habitat conditions from very good to very poor (Figure 6). The UAV RGB orthoimage is also more informative than that

generated from Sentinel-2 imagery. Sentinel-2 did not clearly show the two classes for both indices: poor class (NDVI, >0.2–0.4; GNDV, >0.1–0.3) and very poor class (NDVI, ≤0.2; GNDVI, ≤0.1). It did detect the very good class (NDVI, >0.6–0.7; GNDVI, >0.5–0.6).

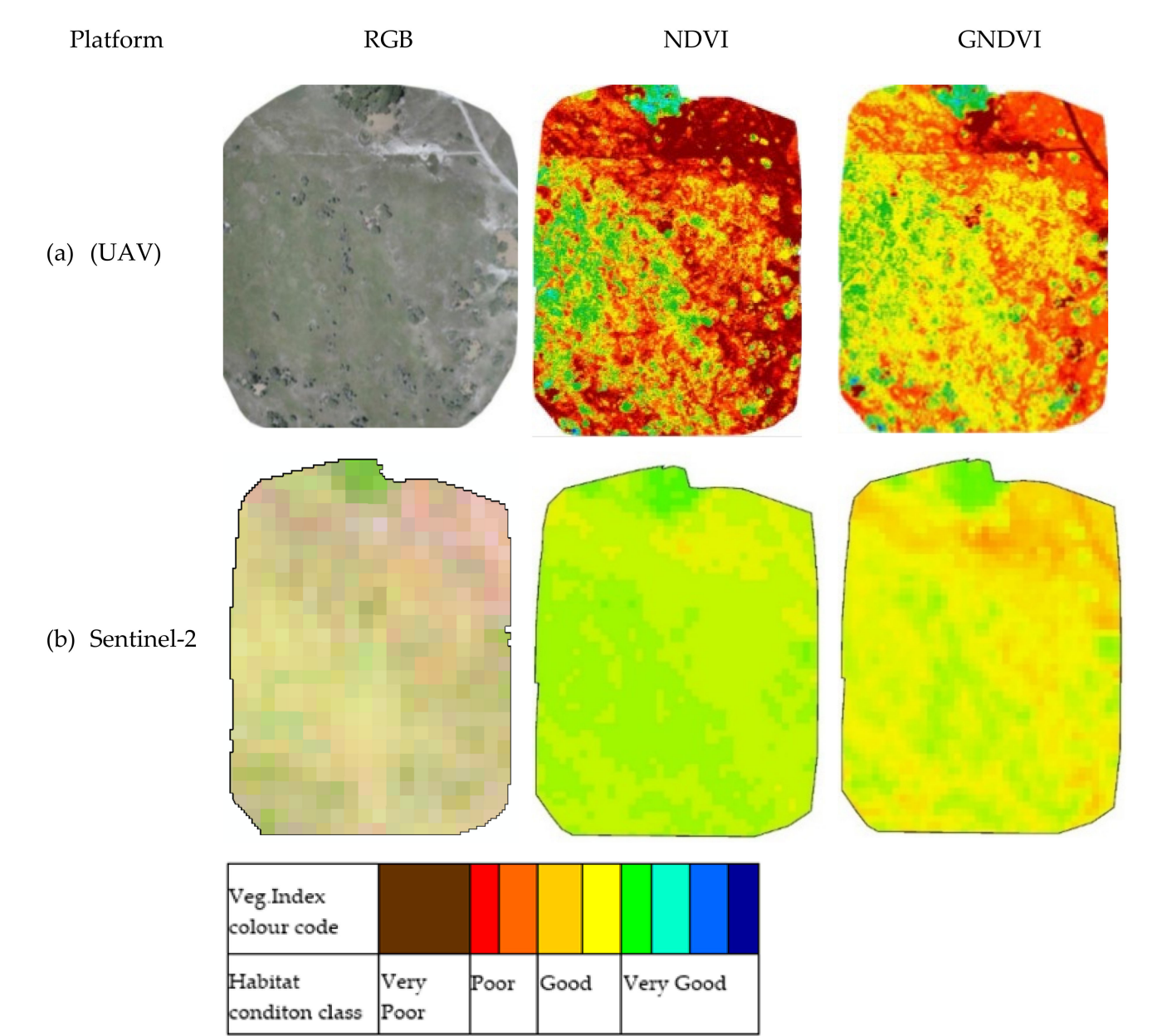**Table 4.** Basic statistics of NDVI values for preliminary indications of habitat conditions in land cover types.

Land Cover Type	Platform	Mean	SD	CV	Skewness	25%	75%	ANOVA F-Test
Grassland	UAV	0.50	0.15	0.30	−0.30	0.40	0.60	$F_{(1,\ 27219)} = 10{,}919$, <0.001
	Sentinel-2	0.30	0.15	0.49	0.34	0.18	0.40	
Mosaic	UAV	0.43	0.11	0.26	0.87	0.35	0.50	$F_{(1,\ 19164)} = 13{,}191$, <0.001
	Sentinel-2	0.23	0.12	0.53	0.85	0.13	0.30	
Riverine	UAV	0.68	0.13	0.20	−0.98	0.60	0.75	$F_{(1,\ 22908)} = 2444$, <0.001
	Sentinel-2	0.59	0.11	0.19	−1.80	0.55	0.66	
Shrubland	UAV	0.55	0.16	0.30	−0.48	0.45	0.70	$F_{(1,\ 38517)} = 7474$, <0.001
	Sentinel-2	0.40	0.12	0.29	−0.11	0.32	0.49	
Woodland	UAV	0.63	0.18	0.29	−0.85	0.50	0.80	$F_{(1,\ 20999)} = 5824$, <0.001
	Sentinel-2	0.44	0.15	0.35	−0.82	0.35	0.55	

Table 5. Basic statistics of GNDVI values for preliminary indications of habitat conditions in land cover types.

Land Cover Type	Platform	Mean	SD	CV	Skewness	25%	75%	ANOVA F-Test
Grassland	UAV	0.47	0.10	0.22	−0.05	0.40	0.55	$F_{(1,\ 22607)} = 516$, $p < 0.001$
	Sentinel-2	0.44	0.13	0.29	−0.05	0.33	0.53	
Mosaic	UAV	0.40	0.10	0.25	0.08	0.35	0.45	$F_{(1,\ 16497)} = 74$, $p < 0.001$
	Sentinel-2	0.38	0.11	0.28	0.42	0.30	0.46	
Riverine	UAV	0.68	0.13	0.20	−0.98	0.60	0.70	$F_{(1,\ 19878)} = 772$, $p < 0.001$
	Sentinel-2	0.66	0.07	0.11	−1.70	0.64	0.71	
Shrubland	UAV	0.55	0.16	0.30	−0.48	0.45	0.55	$F_{(1,\ 37748)} = 208$, $p < 0.001$
	Sentinel-2	0.53	0.09	0.16	−0.23	0.48	0.60	
Woodland	UAV	0.63	0.18	0.29	−0.85	0.50	0.70	$F_{(1,\ 22019)} = 263$, $p < 0.001$
	Sentinel-2	0.56	0.11	0.19	−0.88	0.50	0.64	

3.3. Linear Regression Models for UAV-and Sentinel-2 Vegetation Indices in Land Cover Types

There were strong positive correlations and statistically significant links of the mean values of NDVI generated using the two platforms for each land cover type ($R^2 \geq 0.95$, $p < 0.001$) (Figure 7). The correlations were even higher for GNDVI values generated using the two platforms ($R2 \geq 0.97$, $p < 0.001$) (Figure 8).

Platform	RGB	NDVI	GNDVI

(a) (UAV)

(b) Sentinel-2

Veg.Index colour code								
Habitat conditon class	Very Poor	Poor	Good	Very Good				

Figure 6. Comparative vegetation index maps for NDVI and GNDVI and RGB orthoimages from grassland. The UAV imagery depicts greater detail, obviously, and also provides a much greater range of habitat condition, from very poor to very good.
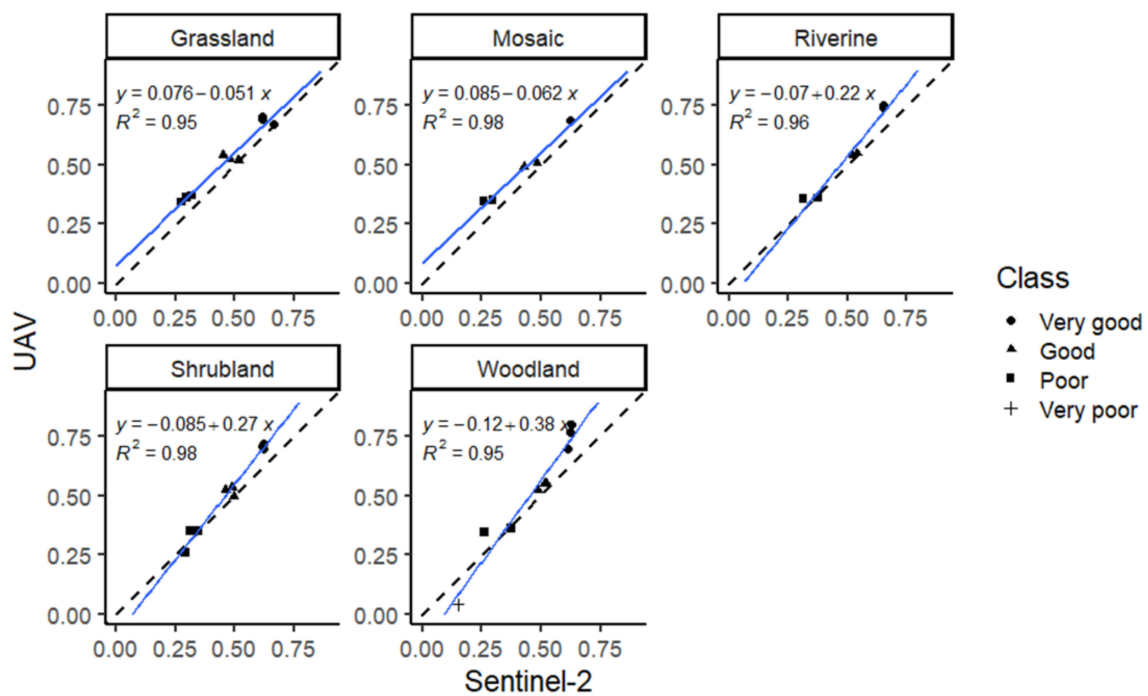
Figure 7. Linear regression between UAV and Sentinel-2 NDVI mean values of different habitat condition classes in each land cover type. In all land cover types, $p < 0.001$.
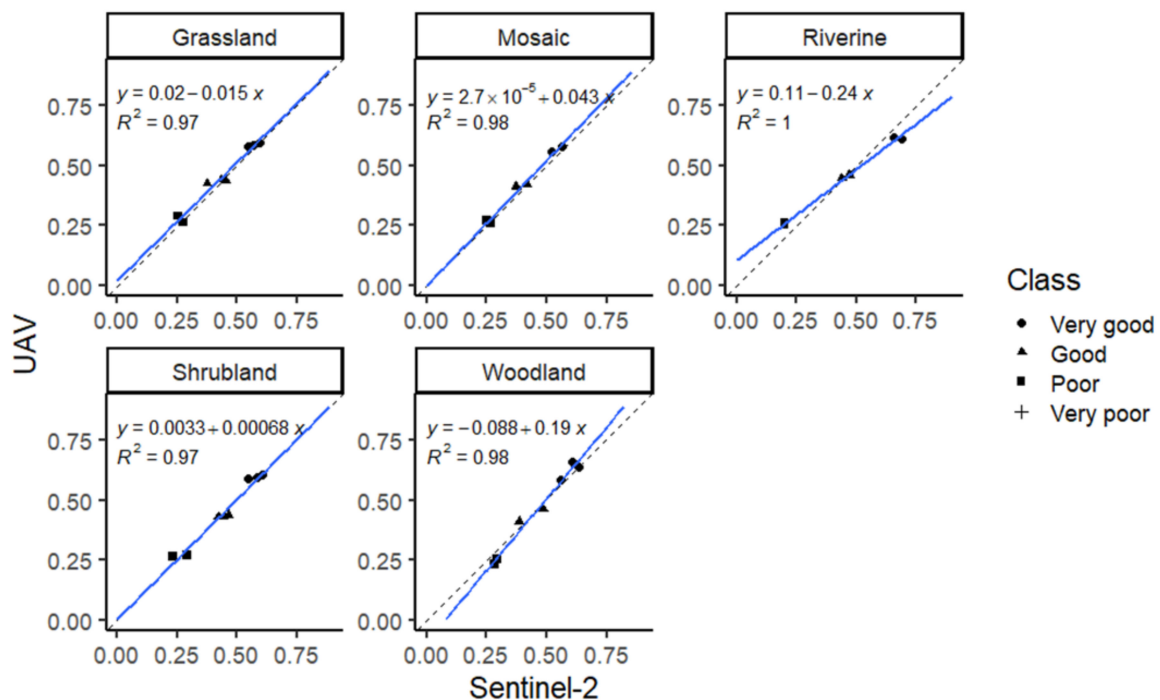
Figure 8. Linear regression between UAV and Sentinel-2 GNDVI mean values of different habitat condition classes in each land cover type. In all land cover types, $p < 0.001$.

4. Discussion

4.1. Comparison Based on Histograms and Basic Statistics of NDVI and GNDVI Values

Our study revealed a higher ability of UAV-based vegetation indices (NDVI and GNDVI) to provide preliminary signals of habitat conditions across land cover types compared to indices derived from the Sentinel-2 platform. With UAV-derived imagery, we

were able to identify a more comprehensive and detailed variation in habitat condition class (from very poor to very good), for both vegetation indices (NDVI and GNDVI) compared to Sentinel-2-derived imagery. In particular, the Sentinel-2-based NDVI seldom detected the habitat in very good condition. The coarser resolution of the satellite imagery results in pixels with values potentially representing the average of several densities of green vegetation as well as bare ground, resulting in a preponderance of moderate values (e.g., Figure 6). Since GNDVI is less likely to saturate at high LAI [31–33], this may explain why we observed more instances of very good conditions using this index. Messina et al. [74] reported similar results in comparing UAV and satellite multispectral imagery in monitoring an onion crop.

Although GNDVI for both UAV and Sentinel-2 platforms showed some similarities across land cover types, those from UAV had a broader variation and greater mean values than the latter (Figure 5b), similar to the results reported by Matese et al. [38]. The wide range of mean values and varying heights of histograms (i.e., frequencies, %) for NDVI and GNDVI reflects habitat heterogeneity [74]. Heterogeneity in land cover types due to varying densities of plant canopies, bare areas, and possibly LAI, are possible explanations for the observed significant differences in the mean values from the two platforms [4,74]. The ability of UAVs to generate more informative histograms related to habitat conditions provides more reliable preliminary insights than the Sentinel-2-based histograms. The results from basic statistics (mean and CV) also showed high statistical differences between the two platforms.

The UAV's higher spatial resolution and low flight altitudes above ground level (AGL), positioning it at a close proximity to plants, were crucial attributes for its observed higher sensitivity in detecting habitat conditions better than the Sentinel-2-sensor [64–66]. The differences in the sensors' spectral properties and atmospheric effects on the vegetation indices (VIs) derived from each platform were additional factors [64]. For example, Sentinel-2-derived NDVI is highly affected by atmospheric conditions [4,34], while UAV-derived VIs are less influenced by atmospheric and solar conditions effects due to the low flight heights and radiometric calibrations. Furthermore, the UAV platform allows data collection in diverse weather conditions, including cloud cover that impairs the quality of satellite imagery and respective vegetation indices [75–77]. On the other hand, data collected from UAV platforms may be impaired under partly cloudy conditions if the sensor and ground surface are experiencing different lighting conditions.

4.2. Comparison Based on Vegetation Index Maps

Qualitative analysis of the vegetation index maps reveals that spatial variation in habitat conditions are more apparent in the UAV-derived NDVI and GNDVI maps than those derived from the Sentinel-2 imageries. For example, all levels of each habitat condition class (very good to very poor) were clearly detected by the UAV platform (Figure 6). In contrast, Sentinel-2 overlooked the poor and very poor classes. These results confirm that UAV-based VI maps can inform and guide wildlife and rangeland managers on specific habitat conditions during the surveyed period. For example, places indicated to have poor and very poor habitat conditions would inform the managers to visit them for the environmental diagnosis of the actual problem and to take appropriate rangeland management interventions and practices.

Statistical test confirmed the higher habitat condition detection capability of UAV-derived NDVI and GNDVIs than Sentinel-2. Similarly, a study conducted in the Kinleith Forest in New Zealand found the UAV platform was more sensitive in detecting health conditions of the forest than the satellite platform [75]. In our study, the statistically significant variations across the classes in each land cover type showed how the UAV-based NDVI and GNDVI maps can better provide useful preliminary signals on habitat condition.

The detailed qualitative information observed in the UAV-based VI maps improve managers' abilities to fulfill near real-time needs in ecological monitoring of wildlife habitats. Such detailed information showing the spatial extent of each habitat condition

class can help wildlife managers and ecologists undertake appropriate wildlife habitats management and improvement. The high-resolution UAV-based patterns can also help assess habitat distribution patterns [77]. Based on the heterogeneous nature of the studied land cover types, the distribution patterns of the habitat condition classes revealed in the index maps reflect the possible abundance, diversity, and distribution patterns of herbivores moving to and utilizing such areas. Several studies support this argument; the variability of vegetation indices, including NDVI and GNDVI, has reliably been used as a proxy for habitat heterogeneity, implying the possible diversity and richness of plant species [78–81]. In turn, habitat heterogeneity in the VI maps suggests the potential richness of mammal species in the area [82,83]. Habitat conditions with adequate forage influence mammals to choose and prefer certain areas [59]. In addition, optimal foraging theory emphasizes that mammals tend to select habitats with a condition that contains the necessary habitat requirements, including foraging patches that ensure high energy return for herbivores [84]. The much-detailed UAV-derived NDVI and GNDVI show higher potential for success in monitoring and managing than those derived from the traditional Sentinel-2 platform. Technologically advanced methods such as the UAV platform are crucial to ensure accurate and timely detection and monitoring of ecological changes in wildlife habitat condition in protected and adjacent areas [78,85,86].

4.3. Comparative Insights from Statistical Correlations and Linear Regressions of NDVI and GNDVI Mean Values Derived by UAV and Sentinel-2

The results revealed strong positive correlations of vegetation indices (NDVI and GNDVI) and mean values derived from the two platforms as preliminary diagnostic signs of habitat condition classes (very good, good, poor, and very poor) in all the land cover types. These results informed the existing link and pattern between the two platforms regarding the NDVI and GNDVI mean values for each land cover type. The high statistical significance levels ($p < 0.001$) generated from linear regressions demonstrated the strong link between UAV and Sentinel-2, for both NDV and GNDVI in each land cover type. Our findings are similar to those of Sozzi et al. [39], although these authors used only NDVI. Our findings were partly attributed to the homogeneity of the habitat condition in the grassland and a more or less uniform mixture of habitat and conditions in the mosaic cover type. Similar correlations between NDVI derived from UAV orthoimages and Sentinel-2 imagery had been recorded in less complex vineyard landscapes of northeastern Italy [24,87].

We have demonstrated the power of vegetation indices derived from very high-resolution UAV-mounted sensors as vital preliminary diagnostic signs of habitat conditions in different land cover types. Since the Sentinel-2 has a lower resolution than the UAV-derived VIs in detecting possible habitat conditions, their integrated applications would generate much more reliable preliminary information on possible habitat conditions in large landscapes.

5. Conclusions

Our study showed a higher sensitivity and ability of UAV-derived vegetation indices (NDVI and GNDVI) than the Sentinel-2 platform for preliminary diagnosis of habitats condition for wild herbivores. Histograms revealed that the UAV detected all habitat condition classes (very good, good, poor, and very poor) at a higher magnitude than Sentinel-2. Spatial distribution patterns of all the classes were more apparent in the UAV-derived vegetation index maps than in the Sentinel-2 based maps. Furthermore, the positive correlations and respective linear regressions between the UAV and Sentinel-2 vegetation indices affirmed a strong link between the two platforms; the former platform outperformed the latter, partly due to its higher spatial resolution and low flight heights above the ground level.

The obtained NDVI and GNDVI preliminary signals of any possible abnormalities regarding habitat conditions would guide wildlife managers and ecologists to quickly get to those sites for timely interventions. The obtained information is a vital input in the ongoing

project for developing the UAV-based ecological monitoring protocol for wildlife habitats in the community wildlife management area. Other potential users of the information include researchers, decision-makers who need real-time data from rapid assessments, and ranch managers and ecologists who would save time and other resources.

Since the UAV technology is relatively new, a broad research project using more than one type and number of UAV is highly needed to test as many vegetation indices as possible for comparative analysis with satellite platforms and ground-based techniques in different land cover types. At least three UAVs are recommended per field mission, two being ready for the operation while the rest would serve as backup.

Appendix A

Table A1. Other vegetation indices that were explored in the literature.

Vegetation Index	Explanations	References
Enhanced Vegetation Index (EVI)	Counteracts atmospheric aerosol and saturation effects, and soil reflectance influence. Its values range between −1 and +1 within which healthy vegetation/forage falls between 0.20 and 0.80. It has a low dynamic range in low vegetated drylands; the C1 and C2 are not needed in UAV-based imagery	[29,31,41–43,70].
Two Band EVI (EVI2)	It avoids signal-to-noise problems and does not need coefficients of aerosol resistance terms (C1 and C2) as those needed in the EVI; hence, it also fits UAV-based VIs computations. This index has a low dynamic range in low vegetated drylands.	[43].
Red Edge NDVI (RENDVI)	As a positive modification of NDVI, it is sensitive to even small changes in vegetation health and enables estimation of available green forage. Its values range from −1 to 1; green vegetation is normally detected from 0.2 to 0.9	[44,45]
Wide Dynamic Range Vegetation Index (WDRVI)	It utilizes the same spectral bands (red and NIR) as that of NDVI. It is at least three times more sensitive to moderate-to-high LAI than that of NDVI; hence, it is also effective in monitoring vegetation states under such moderate-to-high vegetation cover density. Further evaluations of the index had been suggested.	[46]
Atmospherically Resistant Vegetation Index (ARVI)	It's a modification from NDVI; it minimizes atmospheric effects; informs on the state of vegetation, and its values range from −1 to 1 similar to NDVI, RENDVI, and EVI. It has been reported that all vegetation indices designed to reduce atmospheric effect tend to be highly sensitive to the soil reflectance effect; hence, it is not appropriate for arid regions where bare soils predominate. It also has a low dynamic range in low vegetated arid and semi-arid drylands.	[29,88].

References

1. MacDonald, A.; Bartels, S.F.; Macdonald, S.E.; Pigeon, K.E.; MacNearney, D.; Finnegan, L. Wildlife forage cover and composition on pipeline corridors in Alberta: Implications for wildlife conservation. *For. Ecol. Manag.* **2020**, *468*, 118189. [CrossRef]
2. Frair, J.L.; Merrill, E.H.; Visscher, D.R.; Fortin, D.; Beyer, H.L.; Morales, J.M. Scales of movement by elk (*Cervus elaphus*) in response to heterogeneity in forage resources and predation risk. *Landsc. Ecol.* **2005**, *20*, 273–287. [CrossRef]
3. Espach, C.; Lubbe, L.; Ganzin, N. Determining grazing capacity in Namibia with the aid of remote sensing. *Afr. J. Range Forage Sci.* **2009**, *26*, 133–138. [CrossRef]
4. Funghi, C.; Heim, R.H.; Schuett, W.; Griffith, S.C.; Oldeland, J. Estimating food resource availability in arid environments with Sentinel 2 satellite imagery. *PeerJ* **2020**, *8*, e9209. [CrossRef]
5. Ryan, S.; Knechtel, C.; Getz, W. Ecological cues, gestation length, and birth timing in African buffalo (Syncerus caffer). *Behav. Ecol.* **2007**, *18*, 635–644. [CrossRef]
6. Pettorelli, N.; Bro-Jørgensen, J.; Durant, S.M.; Blackburn, T.; Carbone, C. Energy availability and density estimates in African ungulates. *Am. Nat.* **2009**, *173*, 698–704. [CrossRef]
7. Pettorelli, N.; Ryan, S.; Mueller, T.; Bunnefeld, N.; Jędrzejewska, B.; Lima, M.; Kausrud, K. The Normalized Difference Vegetation Index (NDVI): Unforeseen successes in animal ecology. *Clim. Res.* **2011**, *46*, 15–27. [CrossRef]
8. Wilmshurst, J.F.; Fryxell, J.M.; Farm, B.P.; Sinclair, A.; Henschel, C.P. Spatial distribution of Serengeti wildebeest in relation to resources. *Can. J. Zool.* **1999**, *77*, 1223–1232. [CrossRef]
9. Dussault, C.; Courtois, R.; Ouellet, J.-P.; Girard, I. Space use of moose in relation to food availability. *Can. J. Zool.* **2005**, *83*, 1431–1437. [CrossRef]
10. Bukombe, J.; Kittle, A.; Senzota, R.B.; Kija, H.; Mduma, S.; Fryxell, J.M.; Magige, F.; Mligo, C.; Sinclair, A.R. The influence of food availability, quality and body size on patch selection of coexisting grazer ungulates in western Serengeti National Park. *Wildl. Res.* **2019**, *46*, 54–63. [CrossRef]
11. Ranc, N.; Moorcroft, P.R.; Hansen, K.W.; Ossi, F.; Sforna, T.; Ferraro, E.; Brugnoli, A.; Cagnacci, F. Preference and familiarity mediate spatial responses of a large herbivore to experimental manipulation of resource availability. *Sci. Rep.* **2020**, *10*, 1–11. [CrossRef]
12. Lopoukhine, N.; Crawhall, N.; Dudley, N.; Figgis, P.; Karibuhoye, C.; Laffoley, D.; Londoño, J.M.; MacKinnon, K.; Sandwith, T. Protected areas: Providing natural solutions to 21st Century challenges. *SAPI EN. S. Surv. Perspect. Integr. Environ. Soc.* **2012**, *5*, 116–131.

13. Stocking, M.; Murnaghan, N. Land degradation: Guidelines for field assessment. *Overseas Dev. Group Univ. East Angl. Norwich UK* **2000**, *120*, 1–130.

14. Yengoh, G.T.; Dent, D.; Olsson, L.; Tengberg, A.E.; Tucker III, C.J. *Use of the Normalized Difference Vegetation Index (NDVI) to Assess Land Degradation at Multiple Scales: Current status, Future Trends, and Practical Considerations*; Springer: Berlin/Heidelberg, Germany, 2015.

15. Selemani, I.S.; Sangeda, A.Z. Spatial and temporal vegetation dynamics: Opportunities and constraints behind wildlife migration in Eastern Africa Savanna Ecosystem. *Wildl. Manag. Fail. Successes Prospect.* **2019**. [CrossRef]

16. Kideghesho, J.R.; Nyahongo, J.W.; Hassan, S.N.; Tarimo, T.C.; Mbije, N.E. Factors and ecological impacts of wildlife habitat destruction in the Serengeti ecosystem in northern Tanzania. *Afr. J. Environ. Assess. Manag.* **2006**, *11*, 17–32.

17. Wondie, M.; Schneider, W.; Melesse, A.M.; Teketay, D. Spatial and temporal land cover changes in the Simen Mountains National Park, a world heritage site in Northwestern Ethiopia. *Remote Sens.* **2011**, *3*, 752–766. [CrossRef]

18. Di Gregorio, A. *Land Cover Classification System: Classification Concepts and User Manual*; LCCS, FAO: Rome, Italy, 2005; Volume 2.

19. Morgan, B.E.; Chipman, J.W.; Bolger, D.T.; Dietrich, J.T. Spatiotemporal analysis of vegetation cover change in a large ephemeral river: Multi-sensor fusion of unmanned aerial vehicle (uav) and landsat imagery. *Remote Sens.* **2020**, *13*, 51. [CrossRef]

20. Hazarika, M.K.; Honda, K. Estimation of soil erosion using remote sensing and GIS: Its valuation and economic implications on agricultural production. *Sustain. Glob. Farm* **2001**, *1*, 1090–1093.

21. Djuraev, A.; Mirdjalalov, D.; Nuratdinov, A.; Khushvaktov, T.; Karimov, Y. Evaluation of soil salinity level through NDVI in Syrdarya province, Uzbekistan. *Proc. E3S Web Conf.* **2021**, *258*, 03017. [CrossRef]

22. Telesca, L.; Lasaponara, R. Pre-and post-fire behavioral trends revealed in satellite NDVI time series. *Geophys. Res. Lett.* **2006**, *33*. [CrossRef]

23. Candiago, S.; Remondino, F.; De Giglio, M.; Dubbini, M.; Gattelli, M. Evaluating multispectral images and vegetation indices for precision farming applications from UAV images. *Remote Sens.* **2015**, *7*, 4026–4047. [CrossRef]

24. Khaliq, A.; Comba, L.; Biglia, A.; Ricauda Aimonino, D.; Chiaberge, M.; Gay, P. Comparison of satellite and UAV-based multispectral imagery for vineyard variability assessment. *Remote Sens.* **2019**, *11*, 436. [CrossRef]

25. Navarro, J.A.; Algeet, N.; Fernández-Landa, A.; Esteban, J.; Rodríguez-Noriega, P.; Guillén-Climent, M.L. Integration of UAV, Sentinel-1, and Sentinel-2 data for mangrove plantation aboveground biomass monitoring in Senegal. *Remote Sens.* **2019**, *11*, 77. [CrossRef]

26. Carella, E.; Orusa, T.; Viani, A.; Meloni, D.; Borgogno-Mondino, E.; Orusa, R. An Integrated, Tentative Remote-Sensing Approach Based on NDVI Entropy to Model Canine Distemper Virus in Wildlife and to Prompt Science-Based Management Policies. *Animals* **2022**, *12*, 1049. [CrossRef]

27. Soria, J.; Ruiz, M.; Morales, S. Monitoring Subaquatic Vegetation Using Sentinel-2 Imagery in Gallocanta Lake (Aragón, Spain). *Earth* **2022**, *3*, 363–382. [CrossRef]

28. Shamsudeen, M.; Padmanaban, R.; Cabral, P.; Morgado, P. Spatio-Temporal Analysis of the Impact of Landscape Changes on Vegetation and Land Surface Temperature over Tamil Nadu. *Earth* **2022**, *3*, 614–638. [CrossRef]

29. Kawamura, K.; Akiyama, T.; Yokota, H.; Tsutsumi, M.; Yasuda, T.; Watanabe, O.; Wang, G.; Wang, S. Monitoring of forage conditions with MODIS imagery in the Xilingol steppe, Inner Mongolia. *Int. J. Remote Sens.* **2005**, *26*, 1423–1436. [CrossRef]

30. Puliti, S.; Ene, L.T.; Gobakken, T.; Næsset, E. Use of partial-coverage UAV data in sampling for large scale forest inventories. *Remote Sens. Environ.* **2017**, *194*, 115–126. [CrossRef]

31. Huete, A.; Didan, K.; Miura, T.; Rodriguez, E.P.; Gao, X.; Ferreira, L.G. Overview of the radiometric and biophysical performance of the MODIS vegetation indices. *Remote Sens. Environ.* **2002**, *83*, 195–213. [CrossRef]

32. Gitelson, A.; Stark, R.; Grits, U.; Rundquist, D.; Kaufman, Y.; Derry, D. Vegetation and soil lines in visible spectral space: A concept and technique for remote estimation of vegetation fraction. *Int. J. Remote Sens.* **2002**, *23*, 2537–2562. [CrossRef]

33. Wu, W. The generalized difference vegetation index (GDVI) for dryland characterization. *Remote Sens.* **2014**, *6*, 1211–1233. [CrossRef]

34. Gitelson, A.A.; Kaufman, Y.J.; Merzlyak, M.N. Use of a green channel in remote sensing of global vegetation from EOS-MODIS. *Remote Sens. Environ.* **1996**, *58*, 289–298. [CrossRef]

35. Frampton, W.J.; Dash, J.; Watmough, G.; Milton, E.J. Evaluating the capabilities of Sentinel-2 for quantitative estimation of biophysical variables in vegetation. *ISPRS J. Photogramm. Remote Sens.* **2013**, *82*, 83–92. [CrossRef]

36. Moges, S.; Raun, W.; Mullen, R.; Freeman, K.; Johnson, G.; Solie, J. Evaluation of green, red, and near infrared bands for predicting winter wheat biomass, nitrogen uptake, and final grain yield. *J. Plant Nutr.* **2005**, *27*, 1431–1441. [CrossRef]

37. Muir, J.; Robson, A.; Rahman, M. 'Sugar from Space': Using Satellite Imagery to Predict Cane Yield and Variability. In Proceedings of the 40th Conference of the Australian Society of Sugar Cane Technologists (ASSCT 2018), Mackay, Australia, 18–20 April 2018.

38. Matese, A.; Toscano, P.; Di Gennaro, S.F.; Genesio, L.; Vaccari, F.P.; Primicerio, J.; Belli, C.; Zaldei, A.; Bianconi, R.; Gioli, B. Intercomparison of UAV, aircraft and satellite remote sensing platforms for precision viticulture. *Remote Sens.* **2015**, *7*, 2971–2990. [CrossRef]

39. Sozzi, M.; Kayad, A.; Marinello, F.; Taylor, J.; Tisseyre, B. Comparing vineyard imagery acquired from Sentinel-2 and Unmanned Aerial Vehicle (UAV) platform. *Oeno One* **2020**, *54*, 189–197. [CrossRef]

40. Haula, K.; Agbozo, E. A systematic review on unmanned aerial vehicles in Sub-Saharan Africa: A socio-technical perspective. *Technol. Soc.* **2020**, *63*, 101357. [CrossRef]

41. Matsushita, B.; Yang, W.; Chen, J.; Onda, Y.; Qiu, G. Sensitivity of the enhanced vegetation index (EVI) and normalized difference vegetation index (NDVI) to topographic effects: A case study in high-density cypress forest. *Sensors* **2007**, *7*, 2636–2651. [CrossRef]

42. Villamuelas, M.; Fernández, N.; Albanell, E.; Gálvez-Cerón, A.; Bartolomé, J.; Mentaberre, G.; López-Olvera, J.R.; Fernández-Aguilar, X.; Colom-Cadena, A.; López-Martín, J.M. The Enhanced Vegetation Index (EVI) as a proxy for diet quality and composition in a mountain ungulate. *Ecol. Indic.* **2016**, *61*, 658–666. [CrossRef]

43. Mehrotra, N.; Srinivasan, S. Analysing Drone and Satellite Imagery using Vegetation Indices. Available online: https://www.techforwildlife.com/blog/tag/drone (accessed on 17 May 2022).

44. Gitelson, A.; Merzlyak, M.N. Quantitative estimation of chlorophyll-a using reflectance spectra: Experiments with autumn chestnut and maple leaves. *J. Photochem. Photobiol. B Biol.* **1994**, *22*, 247–252. [CrossRef]

45. Sims, D.A.; Gamon, J.A. Relationships between leaf pigment content and spectral reflectance across a wide range of species, leaf structures and developmental stages. *Remote Sens. Environ.* **2002**, *81*, 337–354. [CrossRef]

46. Gitelson, A.A. Wide dynamic range vegetation index for remote quantification of biophysical characteristics of vegetation. *J. Plant Physiol.* **2004**, *161*, 165–173. [CrossRef]

47. URT, The United Republic of Tanzania. *The Wildlife Conservation (Wildlife Management Areas) Regulations*; Ministry of Natural Resources and Tourism, Government Printer: Dar es Salaam, Tanzania, 2012; p. 68.

48. Sumari, N.; Shao, Z.; Huang, M.; Sanga, C.; Van Genderen, J. Urban expansion: A geo-spatial approach for temporal monitoring of loss of agricultural land. In Proceedings of the The International Archives of the Photogrammetry, Remote Sensing and Spatial Information Sciences, 2017 ISPRS Geospatial Week, Wuhan, China, 18–22 September 2017.

49. Sumari, N.S.; Cobbinah, P.B.; Ujoh, F.; Xu, G. On the absurdity of rapid urbanization: Spatio-temporal analysis of land-use changes in Morogoro, Tanzania. *Cities* **2020**, *107*, 102876. [CrossRef]

50. BWMA. *The General Management Plan for Burunge Wildlife Management Area (BWMA): 2010–2020*; Wildlife Division, Ministry of Natural Resources and Tourism: Dar es Salaam, Tanzania, 2010.

51. Prins, H.H.; Loth, P.E. Rainfall patterns as background to plant phenology in northern Tanzania. *J. Biogeogr.* **1988**, *15*, 451–463. [CrossRef]

52. Kicheleri, R.P.; Treue, T.; Kajembe, G.C.; Mombo, F.M.; Nielsen, M.R. Power struggles in the management of wildlife resources: The case of Burunge wildlife management area, Tanzania. In *Wildlife Management-Failures, Successes and Prospects*; IntechOpen: London, UK, 2018.

53. Lee, D.E. Evaluating conservation effectiveness in a Tanzanian community wildlife management area. *J. Wildl. Manag.* **2018**, *82*, 1767–1774. [CrossRef]

54. Oduor, S.O.; Kotut, K. Soda lakes of the East African Rift System: The past, the present and the future. In *Soda Lakes of East Africa*; Springer: Berlin/Heidelberg, Germany, 2016; pp. 365–374.

55. Bonnin, N.; Van Andel, A.C.; Kerby, J.T.; Piel, A.K.; Pintea, L.; Wich, S.A. Assessment of chimpanzee nest detectability in drone-acquired images. *Drones* **2018**, *2*, 17. [CrossRef]

56. Yonah, I.B.; Mourice, S.K.; Tumbo, S.D.; Mbilinyi, B.P.; Dempewolf, J. Unmanned aerial vehicle-based remote sensing in monitoring smallholder, heterogeneous crop fields in Tanzania. *Int. J. Remote Sens.* **2018**, *39*, 5453–5471. [CrossRef]

57. Braun-Blanquet, J. Plant sociology. The study of plant communities. In *Plant Sociology. Study Plant Communities*, 1st ed.; McGraw-Hill Book Co., Inc.: New York, NY, USA; London, UK, 1932.

58. Mangewa , L.J.; Ndakidemi, P.A.; Alward, R.D.; Kija, H.K.; Nasolwa, E.R.; Munishi, L.K. *Advancing Land Use and Land Cover Classification for Conservation using UAV-based Orthoimages: A case of Burunge Wildlife Management Area, Tanzania*; The Nelson Mandela African Institution of Science and Technology: Arusha, Tanzania, 2022.

59. Bergqvist, G.; Wallgren, M.; Jernelid, H.; Bergström, R. Forage availability and moose winter browsing in forest landscapes. *For. Ecol. Manag.* **2018**, *419*, 170–178. [CrossRef]

60. (URT) U.R.o.T. The Civil Aviation (Remotely Piloted Aircraft Systems) Regulations. 2018. Available online: https://www.tcaa.go.tz/ (accessed on 9 March 2021).

61. Cruzan, M.B.; Weinstein, B.G.; Grasty, M.R.; Kohrn, B.F.; Hendrickson, E.C.; Arredondo, T.M.; Thompson, P.G. Small unmanned aerial vehicles (micro-UAVs, drones) in plant ecology. *Appl. Plant Sci.* **2016**, *4*, 1600041. [CrossRef]

62. Franklin, S.E.; Giles, P.T. Radiometric processing of aerial and satellite remote-sensing imagery. *Comput. Geosci.* **1995**, *21*, 413–423. [CrossRef]

63. Chavez, P.S. Image-based atmospheric corrections-revisited and improved. *Photogramm. Eng. Remote Sens.* **1996**, *62*, 1025–1035.

64. Chander, G.; Markham, B.L.; Helder, D.L. Summary of current radiometric calibration coefficients for Landsat MSS, TM, ETM+, and EO-1 ALI sensors. *Remote Sens. Environ.* **2009**, *113*, 893–903. [CrossRef]

65. Young, N.E.; Anderson, R.S.; Chignell, S.M.; Vorster, A.G.; Lawrence, R.; Evangelista, P.H. A survival guide to Landsat preprocessing. *Ecology* **2017**, *98*, 920–932. [CrossRef]

66. Pons, X.; Pesquer, L.; Cristóbal, J.; González-Guerrero, O. Automatic and improved radiometric correction of Landsat imagery using reference values from MODIS surface reflectance images. *Int. J. Appl. Earth Obs. Geoinf.* **2014**, *33*, 243–254. [CrossRef]

67. Ekstrand, S. Landsat TM-based forest damage assessment: Correction for topographic effects. *Photogramm. Eng. Remote Sens.* **1996**, *62*, 151–162.

68. Reed, D.; Anderson, T.; Dempewolf, J.; Metzger, K.; Serneels, S. The spatial distribution of vegetation types in the Serengeti ecosystem: The influence of rainfall and topographic relief on vegetation patch characteristics. *J. Biogeogr.* **2009**, *36*, 770–782. [CrossRef]

69. Gitelson, A.A.; Viña, A.; Arkebauer, T.J.; Rundquist, D.C.; Keydan, G.; Leavitt, B. Remote estimation of leaf area index and green leaf biomass in maize canopies. *Geophys. Res. Lett.* **2003**, *30*. [CrossRef]

70. Huete, A.; Liu, H.; Batchily, K.; Van Leeuwen, W. A comparison of vegetation indices over a global set of TM images for EOS-MODIS. *Remote Sens. Environ.* **1997**, *59*, 440–451. [CrossRef]

71. Maringa, D.; Mugambi, M.; Nathan, G.; Njoka, E.; Ouko, E. Evaluating The Resource Supply Thresholds That Trigger Livestock Movement Leading To Grazing Conflicts In Northern Kenya. *Int. J. Adv. Res. Publications* **2018**, *2*.

72. R Core Team; R Development Core Team. *A Language and Environment for Statistical Computing*; R Foundation for Statistical Computing: Vienna, Austria, 2018.

73. Akoglu, H. User's guide to correlation coefficients. *Turk. J. Emerg. Med.* **2018**, *18*, 91–93. [CrossRef]

74. Messina, G.; Peña, J.M.; Vizzari, M.; Modica, G. A comparison of UAV and satellites multispectral imagery in monitoring onion crop. An application in the 'Cipolla Rossa di Tropea'(Italy). *Remote Sens.* **2020**, *12*, 3424. [CrossRef]

75. Dash, J.P.; Pearse, G.D.; Watt, M.S. UAV multispectral imagery can complement satellite data for monitoring forest health. *Remote Sens.* **2018**, *10*, 1216. [CrossRef]

76. Guo, Y.; Senthilnath, J.; Wu, W.; Zhang, X.; Zeng, Z.; Huang, H. Radiometric calibration for multispectral camera of different imaging conditions mounted on a UAV platform. *Sustainability* **2019**, *11*, 978. [CrossRef]

77. Kedzierski, M.; Wierzbicki, D. Radiometric quality assessment of images acquired by UAV's in various lighting and weather conditions. *Measurement* **2015**, *76*, 156–169. [CrossRef]

78. Song, B.; Park, K. Detection of aquatic plants using multispectral UAV imagery and vegetation index. *Remote Sens.* **2020**, *12*, 387. [CrossRef]

79. Song, H.; Huang, B.; Liu, Q.; Zhang, K. Improving the spatial resolution of landsat TM/ETM+ through fusion with SPOT5 images via learning-based super-resolution. *IEEE Trans. Geosci. Remote Sens.* **2014**, *53*, 1195–1204. [CrossRef]

80. Gould, W. Remote sensing of vegetation, plant species richness, and regional biodiversity hotspots. *Ecol. Appl.* **2000**, *10*, 1861–1870. [CrossRef]

81. Simonson, W.D.; Allen, H.D.; Coomes, D.A. Applications of airborne lidar for the assessment of animal species diversity. *Methods Ecol. Evol.* **2014**, *5*, 719–729. [CrossRef]

82. Kerr, J.T.; Packer, L. Habitat heterogeneity as a determinant of mammal species richness in high-energy regions. *Nature* **1997**, *385*, 252–254. [CrossRef]

83. Onyia, N.N.; Balzter, H.; Berrio, J.-C. Normalized difference vegetation vigour index: A new remote sensing approach to biodiversity monitoring in oil polluted regions. *Remote Sens.* **2018**, *10*, 897. [CrossRef]

84. Charnov, E.L. Optimal foraging, the marginal value theorem. *Theor. Popul. Biol.* **1976**, *9*, 129–136. [CrossRef]

85. De Castro, A.I.; Shi, Y.; Maja, J.M.; Peña, J.M. UAVs for vegetation monitoring: Overview and recent scientific contributions. *Remote Sens.* **2021**, *13*, 2139. [CrossRef]

86. Zhang, X.; Zhang, F.; Qi, Y.; Deng, L.; Wang, X.; Yang, S. New research methods for vegetation information extraction based on visible light remote sensing images from an unmanned aerial vehicle (UAV). *Int. J. Appl. Earth Obs. Geoinf.* **2019**, *78*, 215–226. [CrossRef]

87. Nonni, F.; Malacarne, D.; Pappalardo, S.E.; Codato, D.; Meggio, F.; De Marchi, M. Sentinel-2 Data Analysis and Comparison with UAV Multispectral Images for Precision Viticulture. *Proc. GI Forum* **2018**, *1*, 105–116. [CrossRef]

88. King, M.D.; Kaufman, Y.J.; Menzel, W.P.; Tanre, D. Remote sensing of cloud, aerosol, and water vapor properties from the moderate resolution imaging spectrometer(MODIS). *IEEE Trans. Geosci. Remote Sens.* **1992**, *30*, 2–27. [CrossRef]